AD-A147 483 A QUASI-OPTICAL METHOD FOR MEASURING THE COMPLEX PERMITTIVITY OF MATERIAL..(U) AEROSPACE CORP EL SEGUNDO CA ELECTRONICS RESEARCH LAB F I SHIMABUKURO ET AL. 1/1

UNCLASSIFIED 01 SEP 84 TR-0084(4925-07)-1 SD-TR-84-43 F/G 20/4 NL

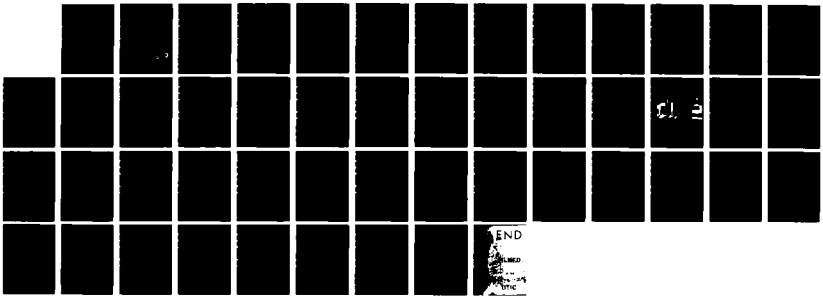

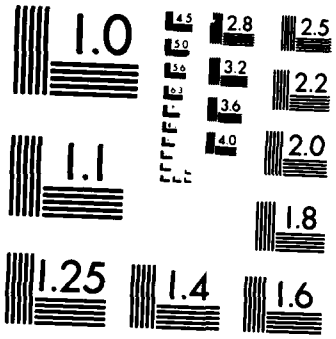

MICROCOPY RESOLUTION TEST CHART
NATIONAL BUREAU OF STANDARDS-1963-A

(12)

REPORT SD-TR-84-43

A Quasi-Optical Method for Measuring the Complex Permittivity of Materials

F. I. SHIMABUKURO, S. LAZAR, and H. B. DYSON
Electronics Research Laboratory
Laboratory Operations
and
M. R. CHERNICK
Concept Development Office
Engineering Group

The Aerospace Corporation
El Segundo, Calif. 90245

AD-A147 483

1 September 1984

APPROVED FOR PUBLIC RELEASE;
DISTRIBUTION UNLIMITED

DTIC
ELECTE
NOV 1 3 1984
S D
E

Prepared for

SPACE DIVISION
AIR FORCE SYSTEMS COMMAND
Los Angeles Air Force Station
P.O. Box 92960, Worldway Postal Center
Los Angeles, California 90009

DTIC FILE COPY

84 11 08 010

This report was submitted by The Aerospace Corporation, El Segundo, CA 90245, under Contract No. F04701-83-C-0084 with the Space Division, P.O. Box 92960, Worldway Postal Center, Los Angeles, CA 90009. It was reviewed and approved for The Aerospace Corporation by D. H. Phillips, Director, Electronics Research Laboratory. Lt Harold J. Morgan, SD/YKX, was the project officer for the Mission Oriented Investigation and Experimentation program.

This report has been reviewed by the Public Affairs Office (PAS) and is releasable to the National Technical Information Service (NTIS). At NTIS, it will be available to the general public, including foreign nationals.

This technical report has been reviewed and is approved for publication. Publication of this report does not constitute Air Force approval of the report's findings or conclusions. It is published only for the exchange and stimulation of ideas.

Harold J. Morgan

HAROLD J. MORGAN, Lt, USAF
Mgr, Space Electronics Division Branch

Joseph Hess

Joseph Hess, GM-15, Director, West Coast Office, AF Space Technology Center

UNCLASSIFIED

SECURITY CLASSIFICATION OF THIS PAGE (When Data Entered)

REPORT DOCUMENTATION PAGE

READ INSTRUCTIONS BEFORE COMPLETING FORM

1. REPORT NUMBER
SD-TR-84-43

2. GOVT ACCESSION NO.

3. RECIPIENT'S CATALOG NUMBER

4. TITLE (and Subtitle)
A QUASI-OPTICAL METHOD FOR MEASURING THE COMPLEX PERMITTIVITY OF MATERIALS

5. TYPE OF REPORT & PERIOD COVERED

6. PERFORMING ORG. REPORT NUMBER
TR-0084(4925-07)-1

7. AUTHOR(s)
Fred I. Shimabukuro, Steven Lazar, Howell B. Dyson, and Michael R. Chernick

8. CONTRACT OR GRANT NUMBER(s)
F04701-83-C-0084

9. PERFORMING ORGANIZATION NAME AND ADDRESS
The Aerospace Corporation
El Segundo, Calif. 90245

10. PROGRAM ELEMENT, PROJECT, TASK AREA & WORK UNIT NUMBERS

11. CONTROLLING OFFICE NAME AND ADDRESS
Space Division
Air Force Systems Command
Los Angeles, Calif. 90009

12. REPORT DATE
1 September 1984

13. NUMBER OF PAGES
40

14. MONITORING AGENCY NAME & ADDRESS(if different from Controlling Office)

15. SECURITY CLASS. (of this report)
Unclassified

15a. DECLASSIFICATION/DOWNGRADING SCHEDULE

16. DISTRIBUTION STATEMENT (of this Report)

Approved for public release; distribution unlimited

17. DISTRIBUTION STATEMENT (of the abstract entered in Block 20, if different from Report)

18. SUPPLEMENTARY NOTES

19. KEY WORDS (Continue on reverse side if necessary and identify by block number)

Dielectric Constant
Millimeter Wave Complex Permittivity
Reflection and Transmission of a Fabry-Perot Plate

20. ABSTRACT (Continue on reverse side if necessary and identify by block number)

A quasi-optical method for measuring the complex permittivity of materials is described. The determination is derived from measurements of the transmission of a perpendicularly polarized wave through a dielectric slab at different angles of incidence. This relatively simple method is quite sensitive and accurate estimates of the relative permittivity and the loss tangent can be obtained by accurately measuring the frequency of the signal

DD FORM (FACSIMILE) 1473

UNCLASSIFIED

SECURITY CLASSIFICATION OF THIS PAGE (When Data Entered)

19. KEY WORDS (Continued)

20. ABSTRACT (Continued)

and by the use of large, precisely machined Fabry-Perot plates. Estimates of the standard errors in the determinations are obtained by using a bootstrap resampling technique. The measurements here were made at a frequency of 93.788 GHz at ambient temperature.

PREFACE

The authors wish to thank G. G. Berry for his help in fabricating components and fixtures for this project.

Accession For
NTIS GRA&I ☒
DTIC TAB ☐
Unannounced ☐
Justification
By
Distribution/
Availability Codes
Dist | Avail and/or Special
A-1

CONTENTS

PREFACE 1

I. INTRODUCTION 9

II. FORMULATION 13

III. EXPERIMENTAL RESULTS 17

IV. DISCUSSION OF RESULTS 31

V. CONCLUSIONS 37

REFERENCES 39

APPENDIX 43

FIGURES

1. In the Measurement Geometry Shown, a Perpendicularly Polarized Wave is Incident on a Dielectric Slab at an Angle θ 15

2. The Reflection Coefficients for Perpendicularly ($r_\perp$) and Parallel ($r_\parallel$) Polarized Waves at a TPX Dielectric Boundary 18

3. The Power Transmission Coefficients Through a 0.498 inch Thick TPX Slab for Perpendicularly and Parallel Polarized Waves 19

4. Photograph of Experimental Setup. The Dielectric Sample is Mounted in Teflon Holder 21

5. The Measured Power Transmission Through a Teflon Slab is Shown by Dots; the Line Curve is $|T_\perp|^2$ Using the Best Fit Estimates of ε_r and tan δ 23

6. The Measured Power Transmission Through a Rexolite Slab is Shown by Dots; the Line Curve is $|T_\perp|^2$ Using the Best Fit Estimates of ε_r and tan δ 24

7. The Measured Power Transmission Through a TPX Slab is Shown by Dots; the Line Curve is $|T_\perp|^2$ Using the Best Fit Estimates of ε_r and tan δ 25

8. The Measured Power Transmission Through a Herasil Slab is Shown by Dots; the Line Curve is $|T_\perp|^2$ Using the Best Fit Estimates of ε_r and tan δ 26

9. The Measured Power Transmission Through a 36D Slab is Shown by Dots; the Line Curve is $|T_\perp|^2$ Using the Best Fit Estimates of ε_r and tan δ 27

10. The Measured Power Transmission Through a 36DA Slab is Shown by Dots; the Line Curve is $|T_\perp|^2$ Using the Best Fit Estimates of ε_r and tan δ 28

11. The Measured Power Transmission Through a 36DK Slab is Shown by Dots; the Line Curve is $|T_\perp|^2$ Using the Best Fit Estimates of ε_r and tan δ 29

12. The Measured Power Transmission Through a 36DS Slab is Shown by Dots; the Line Curve is $|T_\perp|^2$ Using the Best Fit Estimates of ε_r and tan δ 30

TABLES

I. Estimates of Permittivities and Loss Tangents..... 33

II. Comparisons with Other Permittivity Measurements..... 35

I. INTRODUCTION

At the millimeter wavelengths, waveguide, cavity, and various forms of quasi-optical methods are utilized to measure the complex permittivity of materials. Descriptions of the standard methods are given in Ref. 1, and of the modern methods, applicable in the millimeter and sub-millimeter wavelength range, are found in Refs. 2 - 5. Bridges, et al. [6] used two different waveguide measurement techniques to determine the permittivity and loss tangents of materials at 95 GHz: 1) by measuring the transmission through, and reflection from, a dielectric slab in waveguide, taking into account the multiple reflections between surfaces, and 2) by measuring the voltage standing wave ratio (VSWR) of a slab backed by a short, a technique described by Roberts and von Hippel [7]. Open resonators were first used to measure the dielectric properties of materials by Culshaw and Anderson [8], and subsequently by Degenford and Coleman [9]. Balanis [10] determined the permittivity and loss tangent at 60 and 90 GHz by placing a slab in a Fabry-Perot resonator and measuring the resonant spacing and the transmission of the dielectric loaded cavity, and reported errors of less than 1% for ε_r, and ±15% for tan δ. Cullen and Yu [11] developed a theory for measuring permittivity using an open confocal resonator and this formed the basis for more accurate determinations of permittivity. Cook, Jones, and Rosenberg [12] compared cavity and open-resonator measurements of permittivity and loss angle (tangent) at 35 GHz. The agreement between the two methods were well within experimental error. Standard deviations obtained for ε_r and δ were 0.0021 and 2.1 μrad, respectively. Jones [13] further investigated the open resonantor method for measuring dielectrics at 35 GHz and showed that for materials with loss angles in the range of 50-500 μrad, the loss could be

measured with a standard deviation of ± 2% + 1 μrad, and the standard deviation in the determination of relative permittivity was ± 0.1%. In a straightforward quasi-optical method, Talpey [14] determined the complex permittivity of materials with unity permeability at 35.9 GHz by measuring the transmission of a parallel polarized wave through the sample dielectric slab at the Brewster angle. With a coherent source, a Michelson (Ref. 15) or a Mach-Zehnder (Refs. 4, 16) interferometer can be used to measure the relative permittivity, and for low loss materials, this quantity can be measured to a few parts in 10^4 (Ref. 2). Using a broadband source in conjunction with an interferometer, Fourier transform spectrometry can be utilized to derive the permittivity of materials (Ref. 17). Breeden and Shepherd [18] have used this technique in the range of 10-450 GHz to measure the relative permittivity of various materials. They report maximum errors of less than one percent in the determination of the relative permittivity. For broadband applications, the most important method for the determination of the dielectric properties of materials has been dispersive Fourier transform spectrometry (DFTS). This method was first described by Chamberlain, et al. [19] and by Bell [20]. DFTS differs from conventional Fourier transform spectrometry in the positioning of the dielectric sample. In the latter method the sample is placed between the interferometer and the detector. In DFTS the sample is placed in one arm of the interferometer and the ratio of the complex spectra obtained from the transformations of interferograms recorded with and without the sample gives both the attenuation and phase shift caused by the sample. It is seen that a single measurement determines the relative permittivity and loss tangent. Using this method, precise determinations of the complex permittivity of low loss polymers have been made by Birch, et al. [21] and by Afsar, et al. [4]. Errors in the range 0.1% for ε_r, and 2% for tan δ are quoted for the DFTS method.

Waveguide and closed cavity methods use small samples, and the closed systems eliminate diffraction effects and undesirable reflections from extraneous sources. However, at the shorter millimeter wavelengths, precision machining of the slab is required for exact fitting into the waveguide and cavity, and measurement difficulties arise if the wall losses become comparable or exceed the dielectric losses. Quasi-optical methods require large dielectric samples, and care must be exercised to correct for diffraction effects and to eliminate extraneous reflections into the measurement path. However, the method can be extended through the sub-millimeter to optical wavelengths. In this paper we describe a quasi-optical method in which the complex permittivity is determined at 93.788 GHz by measuring the transmission of a perpendicularly polarized wave through a dielectric slab acting as a solid etalon, at different angles of incidence.

II. FORMULATION

The reflection and transmission coefficient of a solid etalon can be calculated by solving a well known boundary value problem. For example, taking into account the complex permittivity and the angular dependence, a derivation is found in [22]. The transmission coefficient of a plane electromagnetic wave through a lossy dielectric slab incident at an angle θ is given by

$$T = \frac{(1-r^2)e^{-j(\beta_1-\beta_o)d}}{1-r^2e^{-2j\beta_1 d}} \tag{1}$$

where

$$\beta_1 = \frac{2\pi}{\lambda_o}\sqrt{\varepsilon_1/\varepsilon_o - \sin^2\theta}$$

$$\beta_o = \frac{2\pi}{\lambda_o}\cos\theta$$

$$\varepsilon_1 = \varepsilon_r\varepsilon_o\left(1 - j\frac{\sigma}{\omega\varepsilon_r\varepsilon_o}\right)$$

and

ε_o = permittivity of free space

ε_r = relative permittivity

σ = conductivity

λ_o = free space wavelength

$\frac{\sigma}{\omega\varepsilon_r\varepsilon_o}$ = tan δ = loss tangent

d = slab thickness

and r is the reflection coefficient of a plane electromagnetic wave incident on a dielectric boundary. For parallel polarization,

$$r = r_{\parallel} = \frac{\beta_1 - (\varepsilon_1/\varepsilon_o)\beta_o}{\beta_1 + (\varepsilon_1/\varepsilon_o)\beta_o} \tag{2}$$

and for perpendicular polarization

$$r = r_{\perp} = \frac{\beta_o - \beta_1}{\beta_o + \beta_1} . \tag{3}$$

For completeness, the slab reflection coefficient is given by

$$R = \frac{r(1-e^{-2j\beta_1 d})e^{2j\beta_o d}}{1-r^2 e^{-2j\beta_1 d}} . \tag{4}$$

The slab power transmission and reflection coefficients are given by $|T|^2$ and $|R|^2$, respectively. A schematic of the experiment is shown in Fig. 1. For the coordinate system shown, the slab is rotated about the y-axis. The zero angle position is determined by auto-collimating a laser beam, co-aligned with the horns, off the slab surface. To insure that angular biases are removed, the transmission measurements are made with the samples rotated clockwise and counter-clockwise and the two readings at each corresponding angle are averaged.

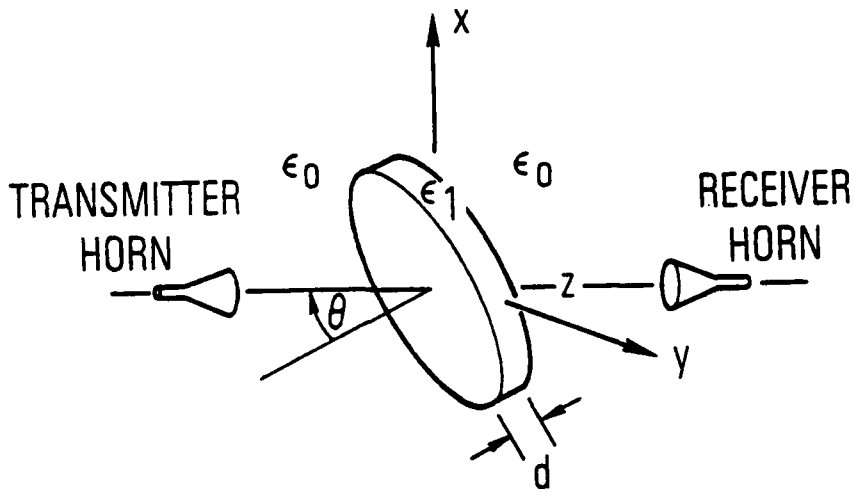

Figure 1. In the measurement geometry shown, a perpendicularly polarized wave is incident on a dielectric slab at an angle θ.

III. EXPERIMENTAL RESULTS

For the transmission experiments described here, a perpendicularly polarized incident wave was transmitted. Off normal incidence $r_\perp$ increases with angle θ, whereas $r_\parallel$ decreases with θ until the Brewster angle, from where it increases to unity at grazing. It is seen that $r_\perp > r_\parallel$ for all angles of incidence. From Equation (1) the contrast, the ratio of an adjacent transmission maximum and minimum, increases with reflectivity and so the use of a perpendicularly polarized wave gives a more accurate measure of the angular position of the transmission peaks and valleys, and thereby that of the real part of the permittivity. As an example, at a frequency of 93.8 GHz, $r_\parallel$ and $r_\perp$ are plotted for a TPX dielectric boundary in Figure 2. In Figure 3 are shown the power transmission coefficients through a 0.498 inch thick TPX sample for both polarizations. For low loss dielectrics the effects of the real part of the permittivity and the loss tangent are almost independent. The loss tangent primarily affects the amplitude level of the slab transmission curve, whereas the relative permittivity determines the angular location of the transmission maxima and minima. An indication of the sensitivity of the measurements is given by the quantities $\frac{\partial |T|^2}{\partial(\tan\delta)}$ and $\frac{\partial\,\theta_{max}}{\partial\,\varepsilon_r}$. For the material TPX above,

$$\frac{\partial |T|^2}{\partial(\tan\delta)}\,(\theta = \theta_{max}) = 40.5 \tag{5}$$

and

$$\frac{\partial\theta_{max}}{\partial\varepsilon_r}\,(\theta = \theta_{max}) = 70, \tag{6}$$

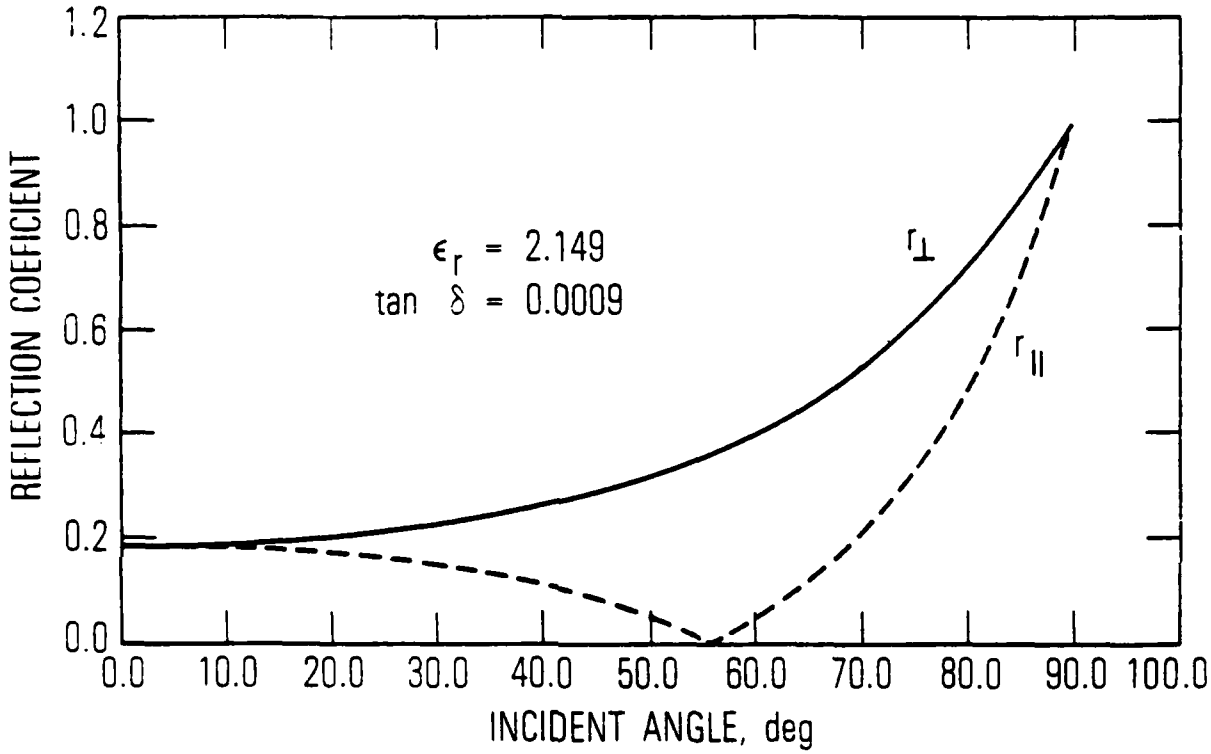

Figure 2. The reflection coefficients for perpendicularly ($r_\perp$) and parallel ($r_\parallel$) polarized waves at a TPX dielectric boundary.

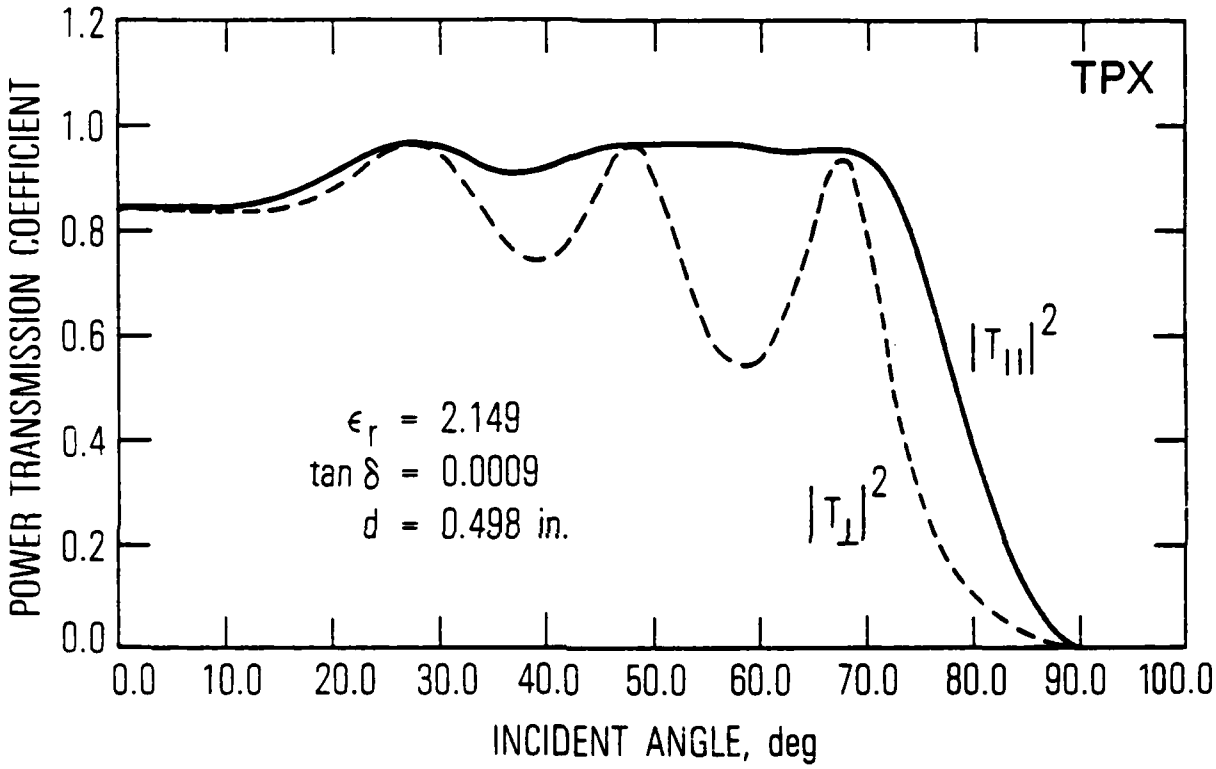

Figure 3. The power transmission coefficients through a 0.498 inch thick TPX slab for perpendicularly and parallel polarized waves.

where θ_{max} is a the angular position of the first transmission maximum. A change of 10^{-3} in the loss tangent changes the peak transmission by 4 percent, and a change of 10^{-2} in the relative permittivity shifts the position of the transmission maximum by 0.7 degree. It is seen that this method has good sensitivity for the measurement of the complex permittivity of materials. A photograph of the essential elements of the experiment is shown in Figure 4. During the actual measurements, pieces of absorbing material were strategically placed around the experiment to eliminate extraneous reflections into the measurement path. The only significantly noticeable extraneous reflections occurred at incident angles near zero degrees and these were due to the multiple reflection interaction between the dielectric sample and the receiving horn. These extraneous reflections increase the standard error in the estimates of the complex permittivity.

The dielectric samples consisted of four inch diameter disks, machined to a flatness ± 0.001 inches on both sides, and ranged in thickness from 0.389 to 0.740 inches. The thickness could be measured to within ± 0.001 inches. The holder for the dielectric samples was fabricated out of teflon and mounted on a precision rotary stage. The angles of incidence were set manually to an estimated accuracy of less than 0.25 degrees. Because of foreshortening effects, useful transmission data could be obtained only to incident angles of about 50 degrees. At that point deleterious reflection effects of the holder could be detected. In the experiment, the power transmission coefficients through the different dielectric slabs were measured at one degree increments of incident angles from 0 to 50 degrees for each of the samples, except for herasil; for this case the transmission measurements were made to a maximum incident angle of 40 degrees. The signal source was a fixed tuned Gunn oscillator whose frequency was measured to less than 1 MHz by down converting into

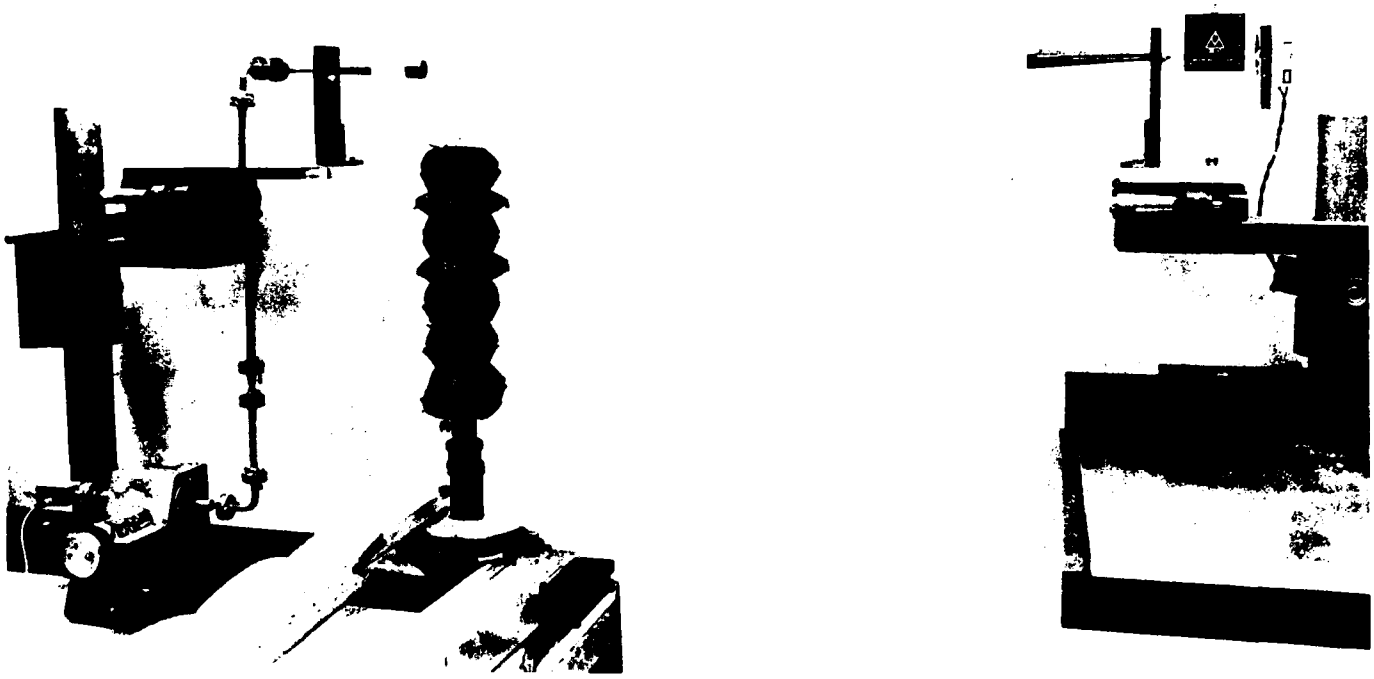

Figure 4. Photograph of experimental setup. The dielectric sample is mounted in the teflon holder.

a frequency counter. The signal frequency drift during the measurements was less than 10 MHz and so the operational wavelength was known to one part in 10^4.

The measured power transmissions of a 93.8 GHz perpendicularly polarized wave at different incident angles through various dielectrics are shown in Figures 5-12. Besides those of the commonly used dielectric materials at the millimeter wavelengths, teflon, rexolite, and TPX, measurements of other reported low-loss dielectric materials are shown. These include herasil, a man-made fused quartz, and several casting resins manufactured by Emerson and Cuming, Inc. The theoretical power transmission curves, $|T|^2$, obtained from Equation (1) are shown along with the measured points. The plotted curves are obtained from the best fit bootstrap estimates which will be discussed in the next section. All measurements are normalized to the signal level without the dielectric; however, the insertion of a dielectric slab into the measurement path increases the power density at the receiving horn. The change in power density depends on the geometry and on the dielectric, and amounted to a few percent correction for the experiments described in this paper. The expression for the correction factor is given in the Appendix. In Figures 5-12, these corrections have been applied to the measured points.

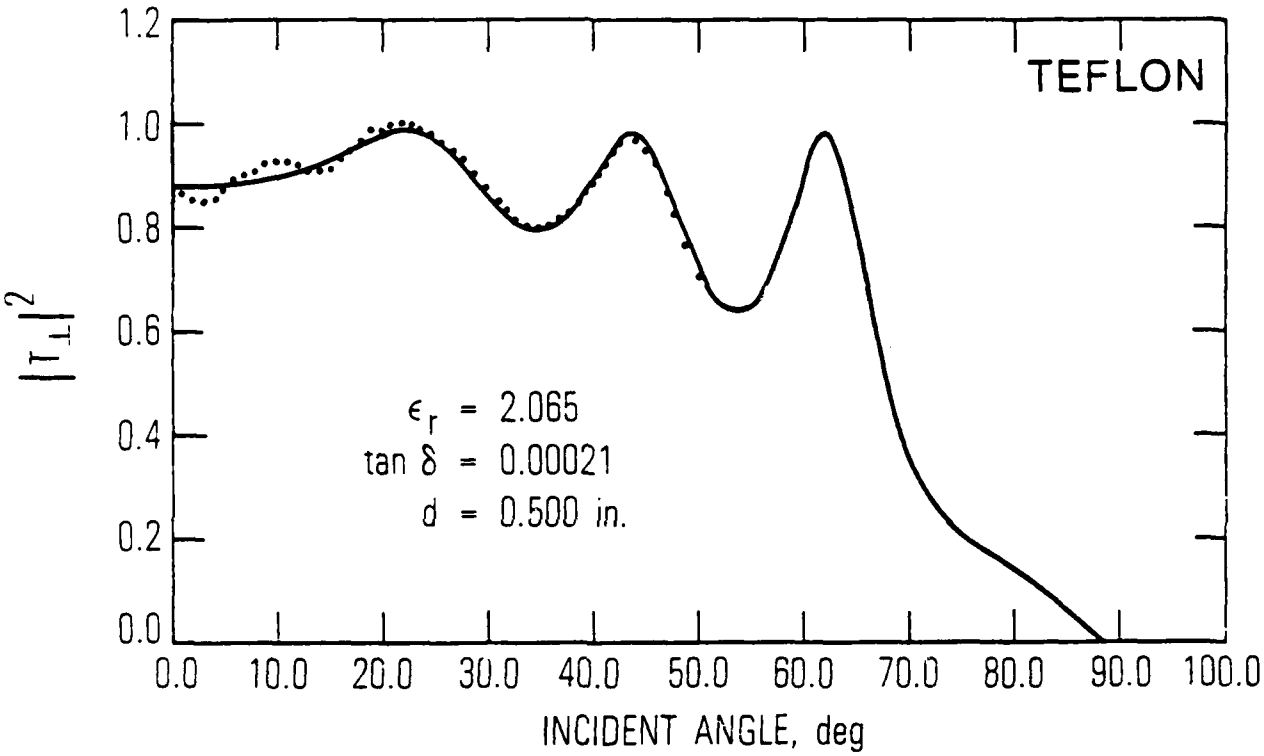

Figure 5. The measured power transmission through a teflon slab is shown by dots. The line curve is $|T_\perp|^2$ using the best fit estimates of ε_r and tan δ.

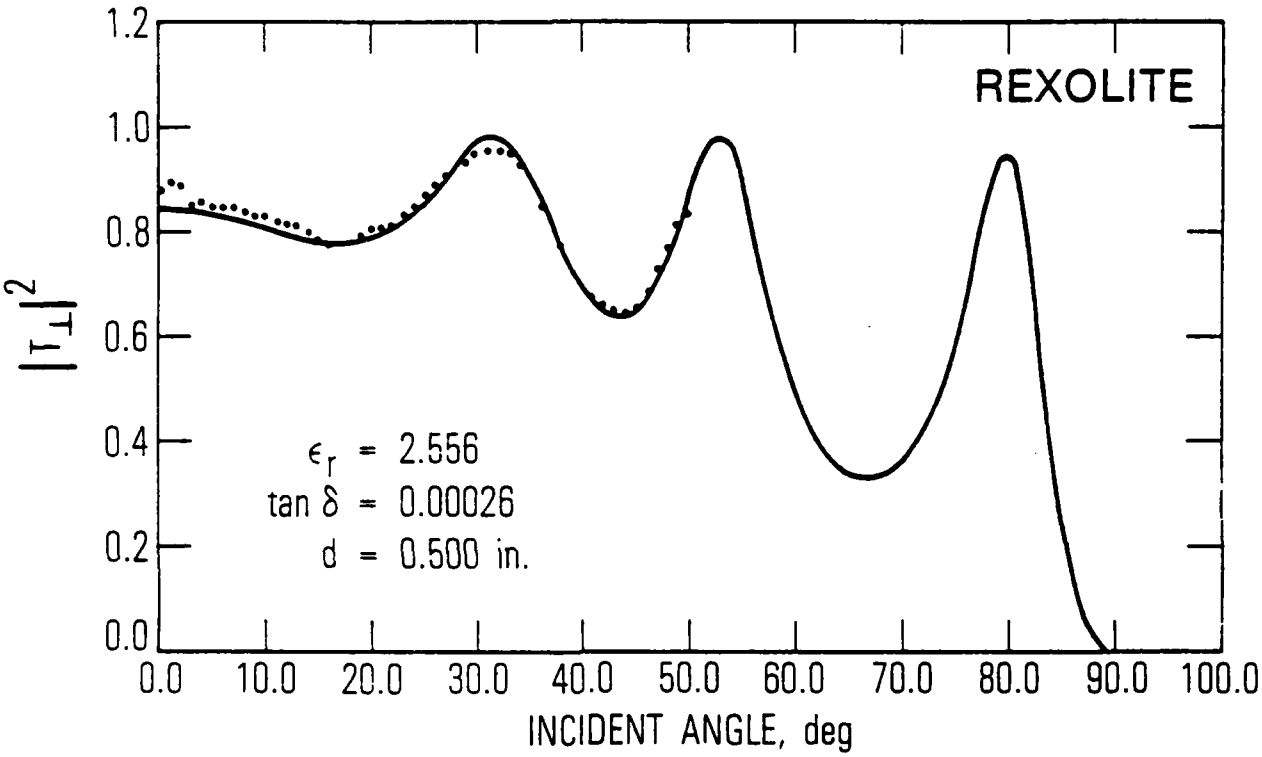

Figure 6. The measured power transmission through a rexolite slab is shown by dots. The line curve is $|T_\perp|^2$ using the best fit estimates of ϵ_r and tan δ.

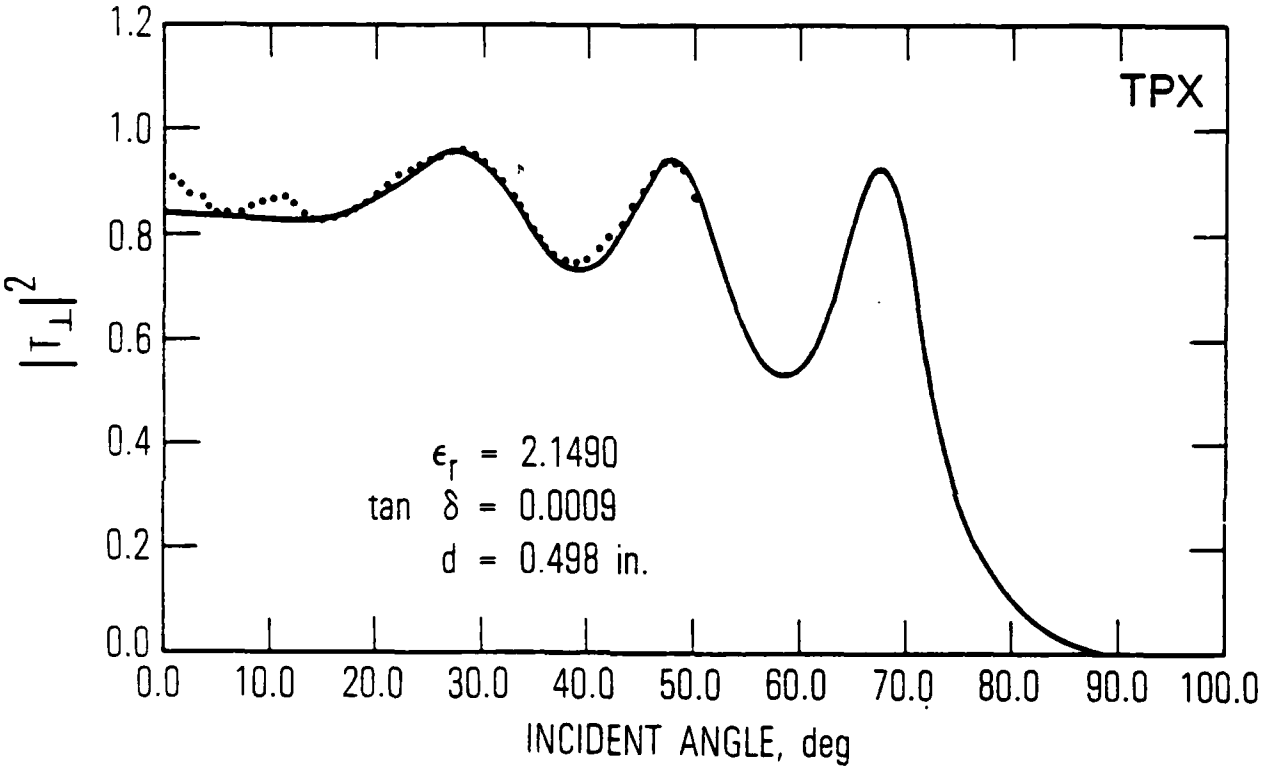

Figure 7. The measured power transmission through a TPX slab is shown by dots. The line curve is $|T_\perp|^2$ using the best fit estimates of ϵ_r and tan δ.

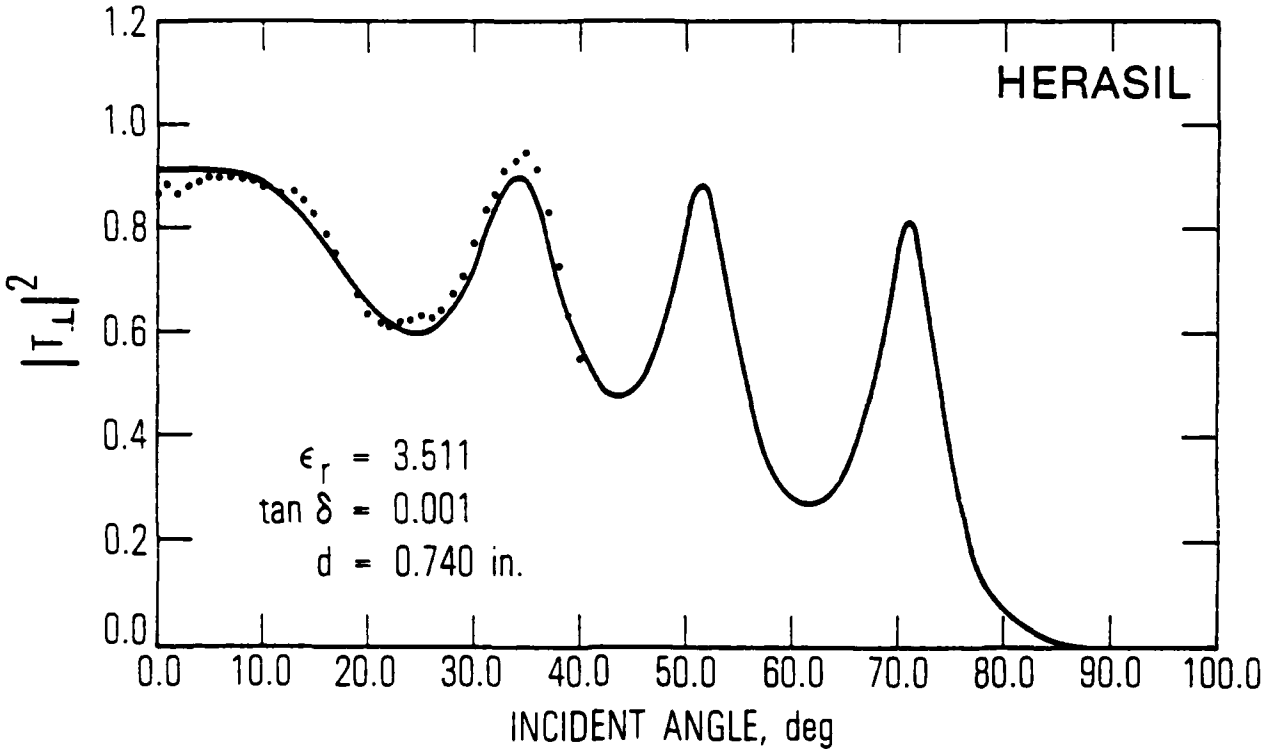

Figure 8. The measured power transmission through a herasil slab is shown by dots. The line curve is $|T_\perp|^2$ using the best fit estimates of ϵ_r and tan δ.

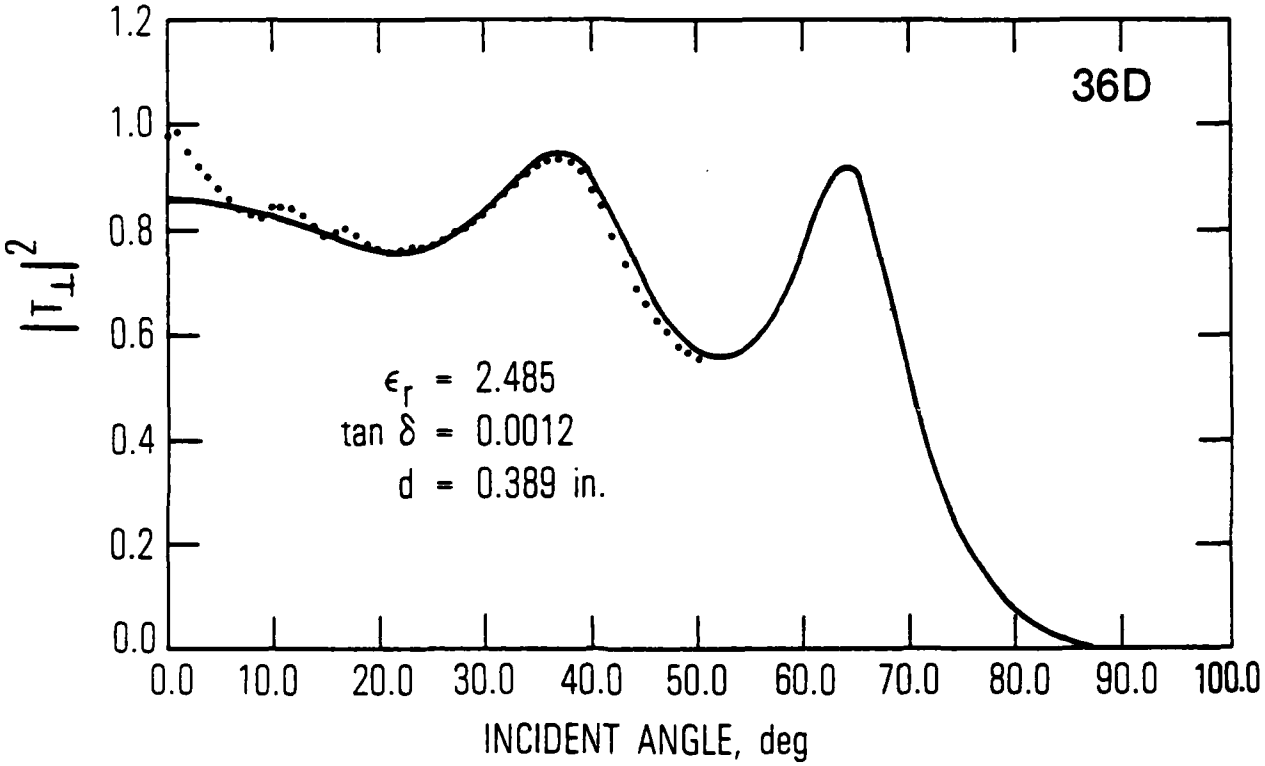

Figure 9. The measured power transmission through a 36D slab is shown by dots. The line curve is $|T_\perp|^2$ using the best fit estimates of ϵ_r and tan δ.

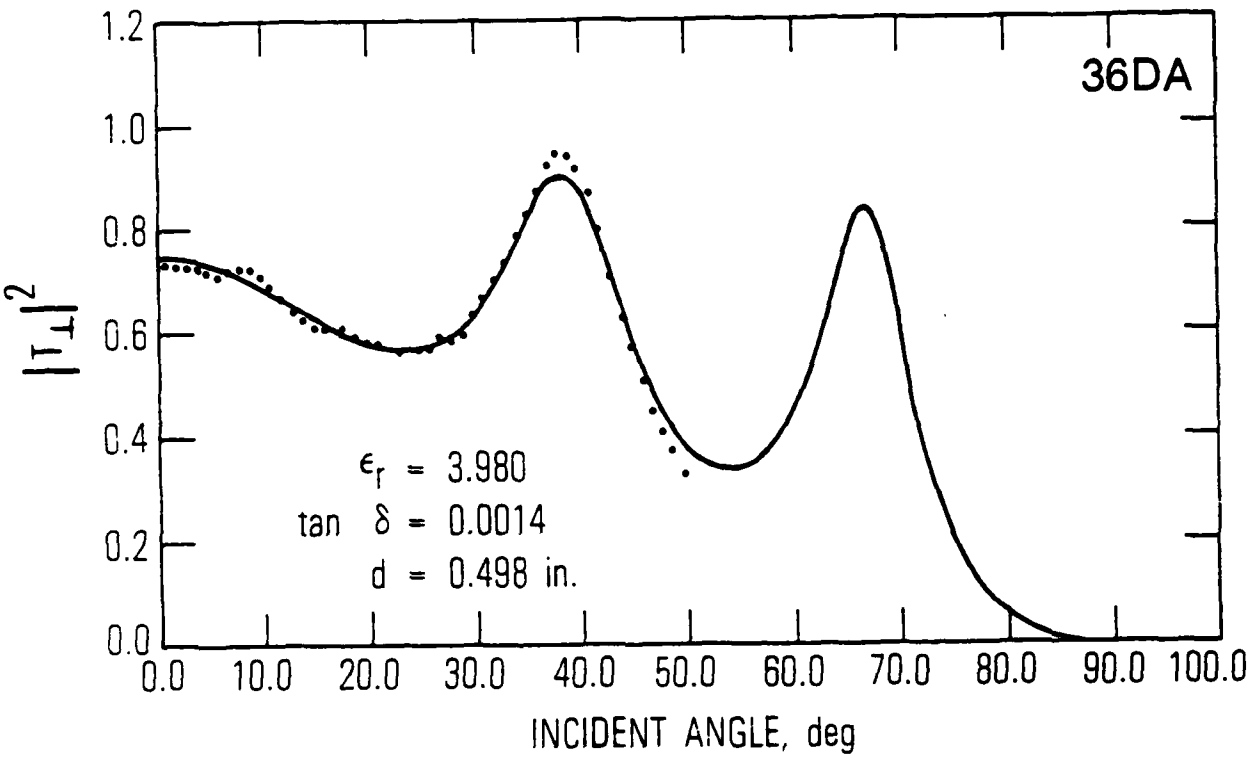

Figure 10. The measured power transmission through a 36DA slab is shown by dots. The line curve is $|T_\perp|^2$ using the best fit estimates of ϵ_r and tan δ.

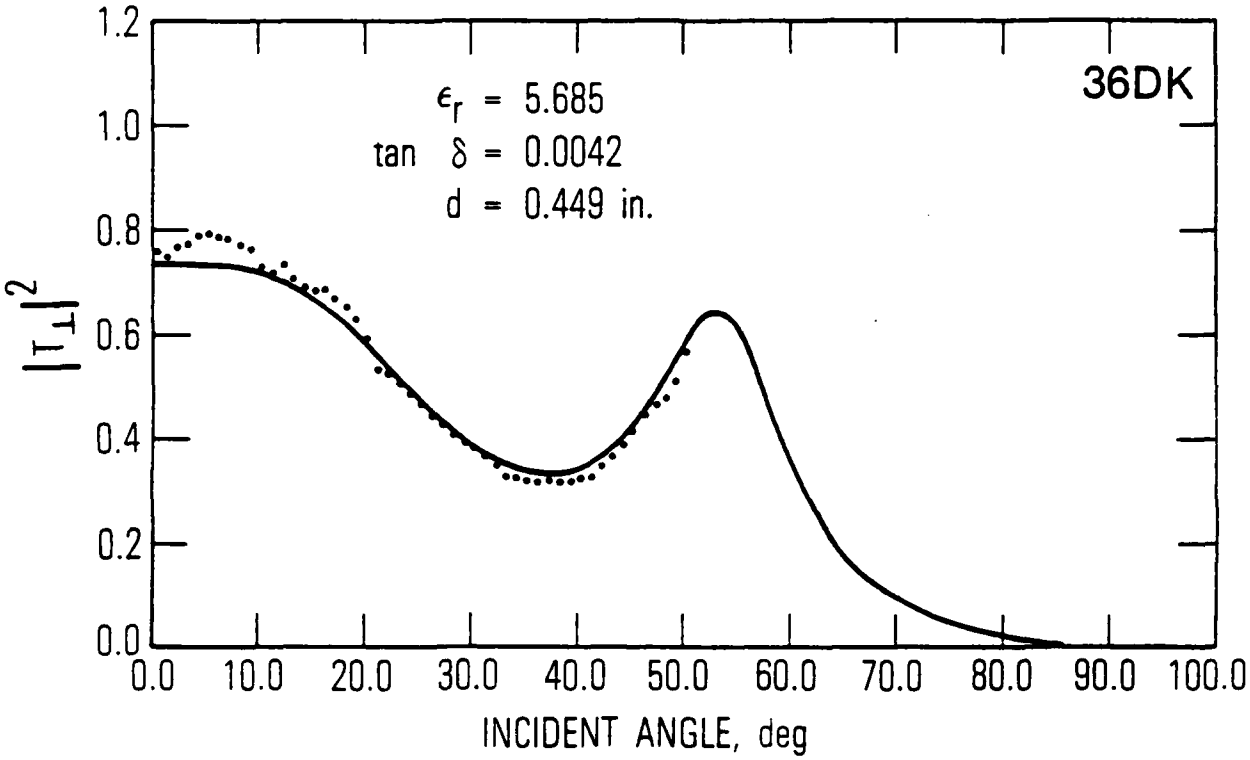

Figure 11. The measured power transmission through a 36DK slab is shown by dots. The line curve is $|T_\perp|^2$ using the best fit estimates of ϵ_r and tan δ.

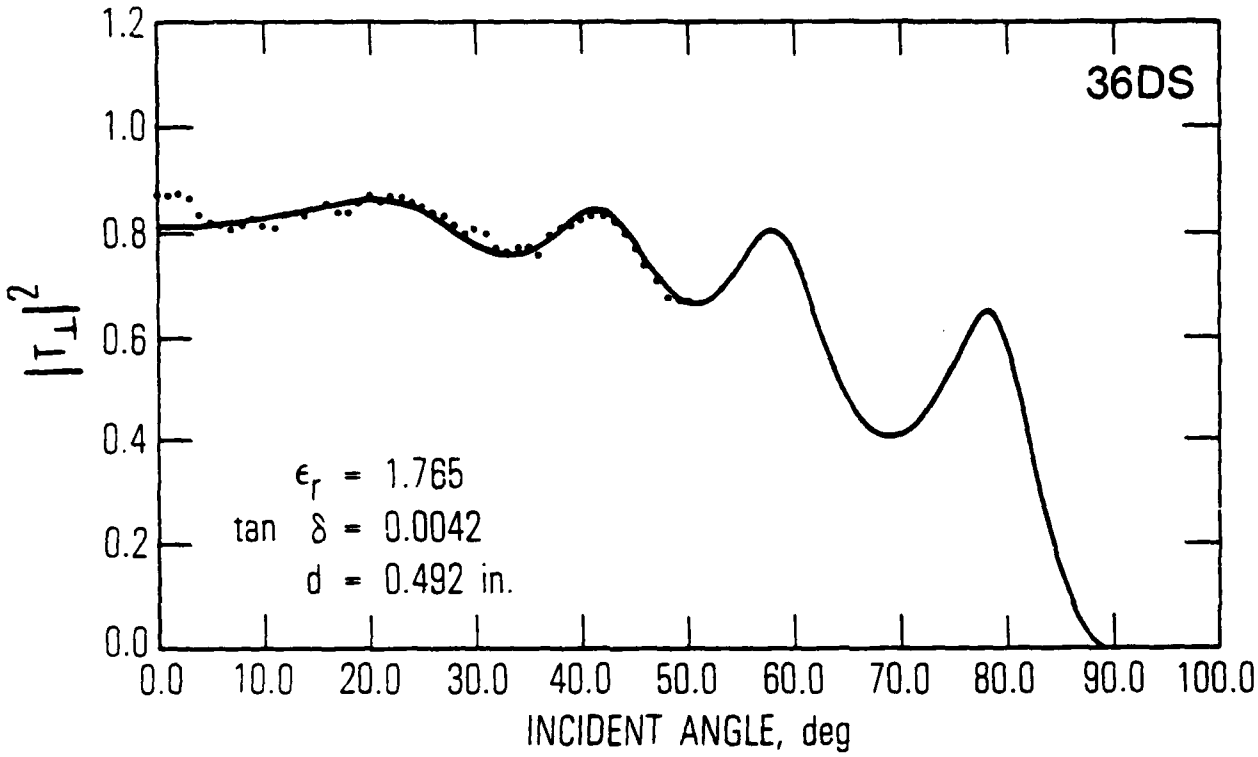

Figure 12. The measured power transmission through a 36DS slab is shown by dots. The line curve is $|T_\perp|^2$ using the best fit estimates of ε_r and tan δ.

IV. DISCUSSION OF RESULTS

The measurement results were analyzed in the following way. The statistical model was assumed to be of the form

$$y_i = g_i(v) + w_i, \; i = 1,2 \ldots N \tag{7}$$

where y_i is the ith power transmission measurement at incident angle θ_i and $\theta_i = i-1$, in degrees. The non-linear function, $g_i(v)$, is the expression $|T|^2$, derived from (1), and v is a vector of two parameters, ε_r (relative permittivity) and tan δ (loss tangent). The wavelength λ, the slab thickness d, and the angle of incidence θ_i are assumed to be known for each observation. The w_i's are the errors and are assumed to be independent and identically distributed from some distribution. There are systematic errors (e.g., near zero incident angle), and the assumption that these errors are random may yield overestimates of the standard errors.

The relative permittivity and the loss tangent are estimated by computing $g_i(v)$ at each i for various trial values of ε_r and tan δ. The values of ε_r and tan δ which minimize

$$S^2 = \frac{1}{51} \sum_{i=1}^{51} (y_i - g_i(v))^2 \tag{8}$$

are taken to be the least squares estimates (for herasil, 41 replaces 51). The residuals are computed for each observation as

$$r_i = y_i - g_i(\hat{v}) \tag{9}$$

where $\hat{v}$ is the least squares estimate of v. The bootstrap technique (Efron, [23]; Efron and Gong, [24]) is then used to estimate the standard error of the least squares estimates of ε_r and tan δ. This is done by the following procedure. A bootstrap sample is generated by

$$y_{bi} = g_i(\hat{v}) + r_{bi}, \; i = 1,2,3\ldots 51 \tag{10}$$

where $r_{bi} = r_j$ with probability $\frac{1}{51}$ for $j = 1,2,\ldots 51$. A bootstrap estimate, $\hat{v}_n$, is obtained for each n by applying the least squares approach to the bootstrap sample. This procedure is replicated B times. B was chosen to be 20 for this application. The bootstrap estimate of v is then

$$\hat{v}_b = \frac{1}{20} \sum_{n=1}^{20} \hat{v}_n \tag{11}$$

and the bootstrap estimate of the covariance matrix is

$$\mathrm{cov}_b = \frac{1}{19} \sum_{n=1}^{20} (\hat{v}_n - \hat{v}_b)(\hat{v}_n - \hat{v}_b)^T \tag{12}$$

where T is the transpose. The estimates of the standard error of the least squares estimates of ε_r and tan δ are obtained directly from cov_b.

Table I gives a summary of the analysis for the dielectrics measured. The materials 36D, 36DA, 36DK, and 36DS are low loss casting resins manufactured by Emerson-Cuming, Inc. The numbers in parentheses for these resins are the permittivities and loss tangents reported by the manufacturer for lower frequencies.

The determination of the real part of the complex permittivity is sensitive to the wavelength and thickness of the dielectric sample, but is

TABLE I

ESTIMATES OF PERMITTIVITIES AND LOSS TANGENTS

f = 93.788 GHz

Material	Least Squares Estimate		Bootstrap Estimates With Standard Error	
	ε_r	tan δ	ε_r	tan δ
Teflon	2.065	0.0002	2.065 ± 0.004	0.00021 ± 0.00003
Rexolite	2.556	0.0003	2.556 ± 0.005	0.00026 ± 0.00006
TPX	2.150	0.0010	2.149 ± 0.005	0.0009 ± 0.0001
Herasil (fused quartz)	3.510	0.0010	3.511 ± 0.005	0.0010 ± 0.0001
36D	2.485 (2.45)	0.0012 (<0.0007)	2.487 ± 0.008	0.0011 ± 0.0002
36DA	3.980 (3.7)	0.0012 (<0.0007)	3.980 ± 0.009	0.0014 ± 0.0001
36DK	5.685 (5.4)	0.0040 (<0.0008)	5.685 ± 0.009	0.0042 ± 0.0001
36DS	1.765 (1.9)	0.0042 (<0.001)	1.766 ± 0.006	0.0041 ± 0.0001

relatively insensitive to errors in the angle of incidence. As mentioned before, the wavelength can be measured very accurately and, in the analysis, it is assumed that this quantity is known exactly. The average of five measured thicknesses was used as the nominal thickness of the dielectric sample, assuming a uniformly distributed error in the range ± 0.001 inch about the nominal value. The uncertainty in the thickness is the largest source of error in estimating the relative permittivity, but in practice, this source of error can be further reduced by fabricating a Fabry-Perot plate to accuracies greater than that obtained in this study. Also, using the best estimate of the nominal thickness reduces the standard errors in Table I for ε_r approximately by a factor of 2. An assumption of a random error of 0.25 degrees rms in the angle measurement has essentially no effect on the results.

The results in Table I show that for the best measurements, the standard errors in the determination of ε_r and tan δ are 0.2% and 2.5%, respectively. The method described in this paper for measuring the complex permittivity of materials is relatively simple, yet, if care is exercised, still gives precisions comparable to the best obtained by other techniques.

In Table II the values of ε_r and tan δ determined in this study are compared with other measurements of the common materials. In the table are listed the reference, the measured permittivities, and the frequencies at which the measurements were made.

TABLE II

COMPARISONS WITH OTHER PERMITTIVITY MEASUREMENTS

Reference	Frequency (GHz)	Material					
		Teflon		Rexolite		TPX	
		ε_r	tan δ	ε_r	tan δ	ε_r	tan δ
This paper	93.8	2.065	0.00021	2.556	0.00026	2.149	0.0009
[6]	94.8	2.04	0.009	2.6	0.0026		
[10]	143	2.07		2.44			
[12]	35*	1.952	0.000048				
[12]	35**	1.956	0.000047				
[13]	34.5	1.950	0.000047			2.126	0.00048
[20]	~120	2.054	0.0008				
[20]	~300					2.1316	0.0016
[21]	~1000					2.1211	0.0127

*open resonator method
**cavity method

V. CONCLUSIONS

Using a quasi-optical method, the complex permittivity of materials can be determined by measuring the power transmission of a perpendicularly polarized wave through a Fabry-Perot etalon fabricated out of the sample dielectric, at different angles of incidence. Accurate determinations are obtained by measuring the signal frequency accurately, and by machining the etalon to close tolerances. Errors due to extraneous reflections into the measurement path are reduced by using large dielectric samples and use of absorbing material at suitable locations. Estimates of the standard errors in the determinations of the relative permittivity and loss tangent are obtained by using a bootstrap resampling technique.

REFERENCES

[1] R. M. Redheffer, "The measurements of dielectric constants," Chap. 10, Technique of Microwave Measurements, C. G. Montgomery, Ed., New York; McGraw-Hill, 1947.

[2] N. W. B. Stone, J. E. Harries, D. W. E. Fuller, J. G. Edwards, A. E. Costley, J. Chamberlain, T. G. Blaney, J. R. Birch, and A. E. Bailey, "Electrical standards of measurement: Part 3: Submillimetre-wave measurements and standards," Proc. IEEE 122, No. 10R, pp. 1054-1070, 1975.

[3] M. J. Bangham, J. R. Birch, T. G. Blaney, A. E. Costley, J. E. Harries, R. G. Jones and N. W. B. Stone, "Physical measurements in the 100-1000 GHz range," Radio and Electron. Engineer 49, pp. 403-417, 1979.

[4] M. N. Asfar, J. Chamberlain, and G. W. Chantry, "High-precision dielectric measurement on liquids and solids at millimeter and submillimeter wavelengths," IEEE Transactions on Instrum. and Meas., IM-25, pp. 290-294, 1976.

[5] M. N. Afsar and K. H. Button, "Precise Millimeter Wave Measurements of Complex Refractive Index, Complex Dielectric Permittivity and Loss Tangent of GaAs, Si, SiO_2, Al_2O_3, BeO, MaCor and Glass," IEEE Trans. Microwave Theory and Tech., MTT 31, pp. 217-223, 1983.

[6] W. B. Bridges, M. B. Klein, and E. Schweig, "Measurement of the dielectric constant and loss tangent of thallium mixed halide crystals KRS-5 and KRS-6 at 95 GHz," IEEE Trans. Microwave Theory Tech (MTT-30), pp. 286-292, March, 1982.

[7] S. Roberts and A. von Hippel, "A new method for measuring dielectric constant and loss in the range of centimeter waves," J. Appl. Phys. 17, pp. 610-616, July 1946.

[8] W. Culshaw and M. V. Anderson, "Measurement of dielectric constants and losses with a millimeter wave Fabry-Perot interferometer," NBS Rept. 8786, 1961.

[9] J. E. Degenford and P. D. Coleman, "A quasi-optics perturbation technique for measuring dielectric constants," Proc. IEEE 54, pp. 520-522, 1966.

[10] C. A. Balanis, "Dielectric constant and loss tangent measurements at 60 and 90 GHz using the Fabry-Perot interferometer," Microwave J. 14, pp. 39-44, 1971.

[11] A. L. Cullen and P. K. Yu, "The accurate measurement of permittivity by means of an open resonator, "Proc. R. Soc. Lond. A. 325, pp. 493-509, 1971.

[12] R. J. Cook, R. G. Jones, and C. B. Rosenberg, "Comparison of cavity and open-resonator measurements of permittivity and loss angle at 35 GHz, "IEEE Trans. on Instrum. and Meas. IM-23, pp. 438-442, 1974.

[13] R. G. Jones, "Precise dielectric measurements at 35 GHz using an open microwave resonator," Proc. IEE, 123, pp. 285-290, 1976.

[14] T. E. Talpey, "Optical methods for the measurement of complex dielectric and magnetic constants at centimeter and millimeter wavelengths," IRE Trans. on Microwave Theory and Tech., MTT-2, pp. 1-12, 1954.

[15] J. E. Chamberlain and H. A. Gebbie, "Determination of the refractive index of a solid using a far infra-red maser," Nature 206, pp. 602-603, 1965.

[16] J. E. Chamberlain, J. Haigh, and M. J. Hine, "Phase modulation in far infrared (submillimeter-wave) interferometers. III - laser refractometry," Infrared Phys. 11, pp. 75-84, 1971.

[17] J. E. Chamberlain, J. E. Gibbs, and H. A. Gebbie, "Refractometry in the far infra-red using a two-beam interferometer," Nature 198, pp. 874-875, 1963.

[18] K. H. Breeden and A. P. Sheppard, "Millimeter and submillimeter wave dielectric measurements," Microwave J., 10, No. 12, pp. 59, 1967.

[19] J. Chamberlain, J. E. Gibbs, and H. A. Gebbie, "The determination of refractive index spectra by Fourier spectrometry," Infrared Phys. 9, pp. 185-209, 1969.

[20] E. E. Bell, "Measurement of the far infrared optical properties of solids with a Michelson interferometer used in the asymmetric mode," Infrared Phys. 6, p. 57-74, 1966.

[21] J. R. Birch, J. D. Dromey, and J. Lesurf, "The optical constants of some common low-loss polymers between 4 and 40 cm^{-1}," Infrared Phys. 21, pp. 225-228, 1981.

[22] D. S. Jones, The Theory of Electromagnetism, Chap. 6, New York, Macmillan, 1964.

[23] B. Efron, The Jackknife, the Bootstrap, and Other Resampling Plans, CBMS-NSF Reg. Conf. Series, Appl. Math 38, Soc. Ind. App. Math, Philadelphia, 1982.

[24] B. Efron and G. Gong, "A leisurely look at the bootstrap, the jackknife, and cross-validation," Amer. Statistician 37, pp. 36-48, 1983.

APPENDIX

In the actual experiment, the incident signal was not a plane wave but a spherical wave. The transmitter and receiver were sufficiently far apart that the calculated results as given by (1) were not affected by the spherical wave. However, the insertion of a dielectric in the ray path increases the power density at the receiver, and the increase in power density has to be taken into account. The change in power density can be calculated in the following way. As viewed geometrically from the transmitter, the receiver horn subtends an angle 2α. With the dielectric slab inserted in the ray path, using ray tracing, ray diverging from the transmitter at an angle slightly greater than 2α now intersect the edges of the receiver horn. If this new angle is called γ, the ratio of the power densities, with and without the dielectric slab is given by the square of the ratio of the subtended angles, $\left(\frac{2\alpha}{\gamma}\right)^2$. If P_o is the power density without the slab, and P_s is that with the slab,

$$\frac{P_o}{P_s} = \left\{1 + \frac{d}{a}\left[\frac{\sin(|\theta-\alpha|-\beta_1)}{\cos\alpha\,\cos\beta_1} - \frac{\sin(\theta+\alpha-\beta_2)}{\cos\alpha\,\cos\beta_2}\right]\right\}^{-2}$$

where

$$\beta_1 = \sin^{-1}\left[\frac{\sin(\theta-\alpha)}{n}\right]$$

$$\beta_2 = \sin^{-1}\left[\frac{\sin(\theta+\alpha)}{n}\right]$$

$n = \sqrt{\varepsilon_r}$, the index of refraction of the dielectric sample

and

θ = angle of incidence for the axial ray

2α = geometric angle subtended by receiver horn as viewed from transmitter horn

a = receiver horn dimension

d = thickness of dielectric slab

U.S. GOVERNMENT PRINTING OFFICE: 1984 584-070

LABORATORY OPERATIONS

The Laboratory Operations of The Aerospace Corporation is conducting experimental and theoretical investigations necessary for the evaluation and application of scientific advances to new military space systems. Versatility and flexibility have been developed to a high degree by the laboratory personnel in dealing with the many problems encountered in the nation's rapidly developing space systems. Expertise in the latest scientific developments is vital to the accomplishment of tasks related to these problems. The laboratories that contribute to this research are:

Aerophysics Laboratory: Launch vehicle and reentry aerodynamics and heat transfer, propulsion chemistry and fluid mechanics, structural mechanics, flight dynamics; high-temperature thermomechanics, gas kinetics and radiation; research in environmental chemistry and contamination; cw and pulsed chemical laser development including chemical kinetics, spectroscopy, optical resonators and beam pointing, atmospheric propagation, laser effects and countermeasures.

Chemistry and Physics Laboratory: Atmospheric chemical reactions, atmospheric optics, light scattering, state-specific chemical reactions and radiation transport in rocket plumes, applied laser spectroscopy, laser chemistry, battery electrochemistry, space vacuum and radiation effects on materials, lubrication and surface phenomena, thermionic emission, photosensitive materials and detectors, atomic frequency standards, and bioenvironmental research and monitoring.

Electronics Research Laboratory: Microelectronics, GaAs low-noise and power devices, semiconductor lasers, electromagnetic and optical propagation phenomena, quantum electronics, laser communications, lidar, and electro-optics; communication sciences, applied electronics, semiconductor crystal and device physics, radiometric imaging; millimeter-wave and microwave technology.

Information Sciences Research Office: Program verification, program translation, performance-sensitive system design, distributed architectures for spaceborne computers, fault-tolerant computer systems, artificial intelligence, and microelectronics applications.

Materials Sciences Laboratory: Development of new materials: metal matrix composites, polymers, and new forms of carbon; component failure analysis and reliability; fracture mechanics and stress corrosion; evaluation of materials in space environment; materials performance in space transportation systems; analysis of systems vulnerability and survivability in enemy-induced environments.

Space Sciences Laboratory: Atmospheric and ionospheric physics, radiation from the atmosphere, density and composition of the upper atmosphere, aurorae and airglow; magnetospheric physics, cosmic rays, generation and propagation of plasma waves in the magnetosphere; solar physics, infrared astronomy; the effects of nuclear explosions, magnetic storms, and solar activity on the earth's atmosphere, ionosphere, and magnetosphere; the effects of optical, electromagnetic, and particulate radiations in space on space systems.

END

FILMED

12-84

DTIC